Hydrated sub-are mantle: A source for the Kluchevskoy volcano, Kamchatka/Russia

3 authors, including:

Frank Dorendorf
Georg-August-Universität Göttingen
17 PUBLICATIONS **928** CITATIONS

SEE PROFILE

Gerhard Wörner
Georg-August-Universität Göttingen
261 PUBLICATIONS **8,180** CITATIONS

SEE PROFILE

Some of the authors of this publication are also working on these related projects:

Project Geology of the central andes in northern Chile View project

Project Trace element determination via high sensitivity Laser Ablation Sector Field ICP-MS View project

Hydrated sub-arc mantle: a source for the Kluchevskoy volcano, Kamchatka/Russia

Frank Dorendorf [a], Uwe Wiechert [a,b,1], Gerhard Wörner [a],*

[a] *Geochemisches Institut, University of Göttingen, Goldschmidtstr. 1, 37077 Göttingen, Germany*
[b] *Geophysical Laboratory, Carnegie Institiution of Washington, 5251 Broad Branch Rd. NW, Washington, DC 20015, USA*

Abstract

Oxygen isotope ratios of olivine and clinopyroxene phenocrysts from the Kluchevskoy volcano in Kamchatka have been studied by CO_2 and ArF laser techniques. Measured $\delta^{18}O$ values of 5.8–7.1‰ for olivine and 6.2–7.5‰ for clinopyroxene are significantly heavier than typical mantle values and cannot be explained by crustal assimilation or a contribution of oceanic sediments. Positive correlations between $\delta^{18}O$ and fluid-mobile elements (Cs, Li, Sr, Rb, Ba, Th, U, LREE, K) and a lack of correlation with fluid-immobile elements (HFSE, HREE) suggest that ^{18}O was introduced into the mantle source by a fluid from subducted altered oceanic basalt. This conclusion is supported by radiogenic isotopes (Sr, Nd, Pb). Mass balance excludes simple fluid-induced mantle melting. Instead, our observations are consistent with melting a mantle wedge which has been hydrated by ^{18}O-rich fluids percolating through the mantle wedge. ^{18}O-enriched fluids are derived from the subducted oceanic crust and the Emperor seamount chain, which is responsible for a particularly high fluid flux. This hydrated mantle wedge was subsequently involved in arc magmatism beneath Kluchevskoy by active intra-arc rifting. © 2000 Elsevier Science B.V. All rights reserved.

1. Introduction

Arc magmatism is triggered by lowering the solidus in the mantle wedge through ingress of slab-derived fluids. The mantle wedge is the main source of subduction zone magmatism, but

---

* Corresponding author. Tel.: +49-551-393971/72;
Fax: +49-551-393982; E-mail: gwoerne@gwdg.de

[1] Present address: Institute for Isotope Geology and Mineral Resources, ETH-Zentrum, Sonneggstr. 5, CH-8092 Zürich, Switzerland.

a significant contribution of trace elements comes from subducted sediments and/or fluids from altered oceanic crust. It has been shown [1] that some trace element abundances in depleted arc magmas are correlated with the specific subduction fluxes beneath arcs and Sr and Be isotopes to permit tracing and quantification of sediment fluxes into the wedge source. More controversial is the nature and amount of the slab fluid. Recent estimations range from less than 1% [2] to values up to 20% [3]. These differences stem from limited knowledge of fluid composition and the nature of interaction with the mantle.

Oxygen isotopes are a powerful tool for tracing

crustal material in basalts [4]. This assumes the mantle oxygen isotope composition to be constant [5] and that rocks studied represent magmatic O isotope values. Glasses and/or feldspar in whole rock samples are very sensitive to alteration and mafic minerals have been difficult to analyze conventionally. However, new laser ablation techniques have been developed and give reliable O isotope compositions on olivine and pyroxene [6]. The accepted range of O isotope composition for mantle rocks based on these studies is $5.7 \pm 0.5\%$ (2σ) relative to SMOW [7]. Previous work [8,9] reported conventional $\delta^{18}O$ data and elevated values for Kluchevskaya group lavas in the Central Kamchatka, the implications of which have been controversial.

We present new ArF and CO_2 laser ablation oxygen isotope data for olivine and clinopyroxene phenocrysts from a suite of 16 basalts and basaltic andesites from the Holocene Kluchevskoy volcano. Our results exclude alteration and problems with Mg-rich samples in conventional studies. In addition, the high precision of our data shows $\delta^{18}O$ to be closely correlated with some major and trace elements and Sr and Pb isotopes. From these correlations we show that the source of the ^{18}O-enriched oxygen is hydrothermally altered oceanic crust introduced by source contamination rather than assimilation of arc crust. We argue for a special role of the subducted Emperor seamount chain and Quaternary intra-arc rifting in Kamchatka.

2. Geological setting and sampling

Quaternary volcanism on Kamchatka in Far Eastern Russia is related to the subduction (9 cm/yr) of the Pacific below the Eurasian plate. Volcanic centers are concentrated in three zones parallel to the trench (Fig. 1A): (1) the Eastern Volcanic Front (EVF), (2) the Central Kamchatka Depression (CKD) and (3) the western Sredinny range (SR). The EVF consists of about 20 active and many more Holocene to Pleistocene volcanoes. Quaternary volcanism in the SR is of
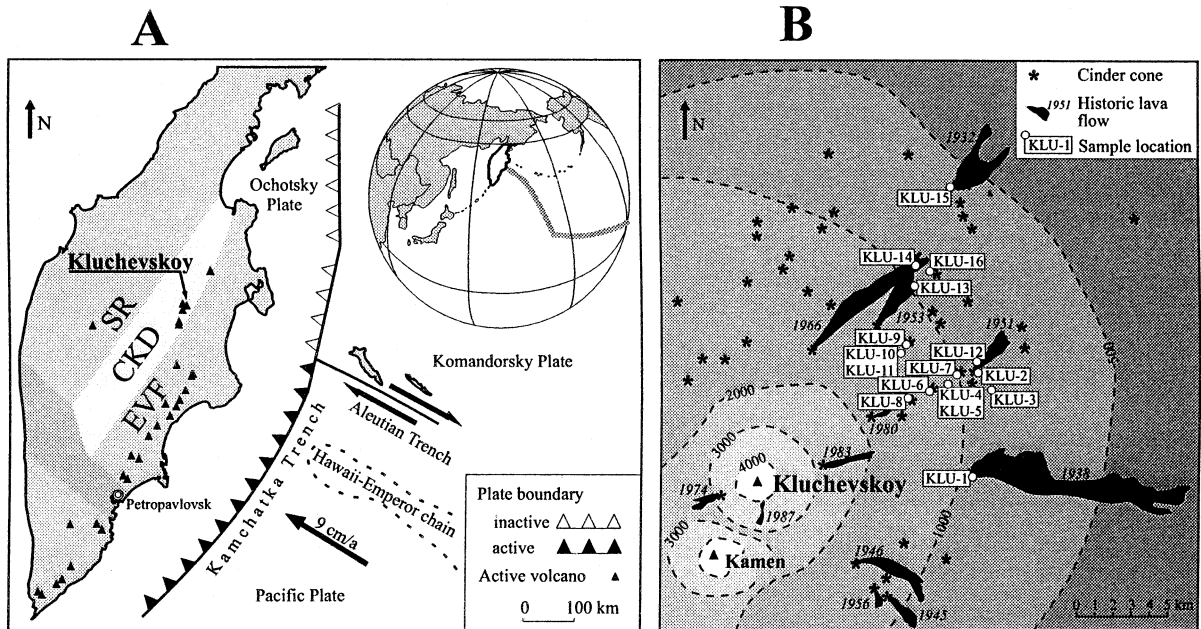

Fig. 1. (A) Kamchatka Peninsula, tectonic structure and active volcanism in the Eastern Volcanic Front (EVF), Central Kamchatka Depression (CKD) and Sredinny Ridge (SR). Modified after [12]. (B) Cinder cones, historic eruptions and sample locations at Kluchevskoy volcano.
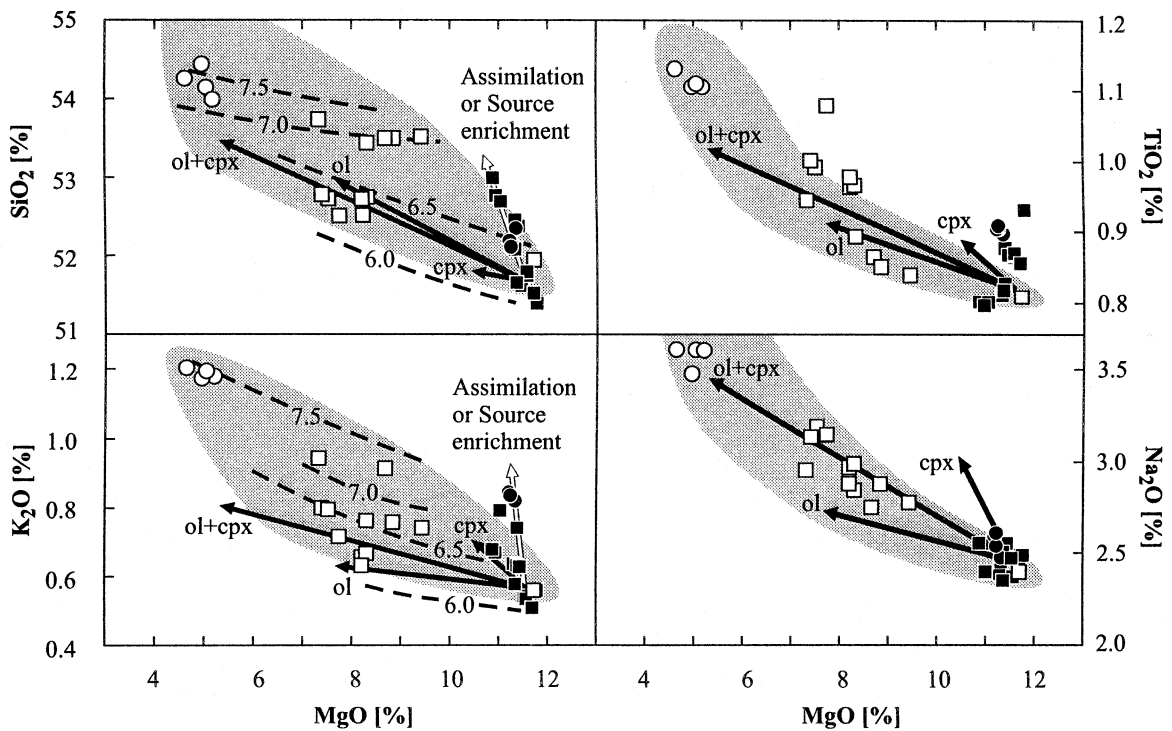
Fig. 2. Plots of MgO versus SiO_2, TiO_2, K_2O and Na_2O for Kluchevskoy samples. HMB and HAB are distinguished by open squares and circles, respectively. Closed symbols are calculated fractionation-corrected, primitive compositions for Mg#70. Vectors for 10% olivine (ol), 20% clinopyroxene (cpx) and 10% olivine+20% clinopyroxene (ol+cpx) fractionation are shown in each diagram. It is obvious from MgO–K_2O–SiO_2 and trace element relations that additional processes other than fractional crystallization are necessary to explain the compositional range. Dashed lines in the plots of MgO versus SiO_2 and K_2O represent contours of $\delta^{18}O$ (‰). The gray field represents the data for Kluchevskoy of [10].

the back arc type. The Kluchevskaya Group in the CKD, which represents a 200 km wide graben structure, comprises 12 volcanoes all less than 50 000 years old. The largest and highest is the recently active Holocene Kluchevskoy volcano (4750 m), one of the most productive arc volcanoes in the world. Eruption products are high-Mg basalts and basaltic andesites (HMB) and high-Al basaltic andesites (HAB). This suite is explained by polybaric fractionation under hydrous conditions starting at 19 kbar and 1350°C [10,11]. High magmatic water contents suppress plagioclase crystallization resulting in strong Al_2O_3 enrichment in the melt.

Geophysical studies show that Cenozoic volcanic deposits extend to 8 km below Kluchevskoy volcano [12]. Greenschist to amphibolite facies

rocks of Mesozoic (?) age constitute the crust mantle down to 30 km. A funnel-like zone of magma ascent between 20 and 50 km connects the Kluchevskaya group volcanoes with their mantle source [13]. The top of the Wadati–Benioff zone below Kluchevskoy is at a depth of about 160 km [12].

Samples studied here were on the NE and N base of Kluchevskoy (Fig. 1B, **EPSL Online Background Dataset**[2] Table 1). The historic samples are HMB from the eruptions of 1932 and 1938 and HAB from the eruptions of 1951, 1953 and 1956. The remaining samples (all HMBs)

---

[2] http://www.elsevier.nl/locate/epsl; mirrorsite: http://www.elsevier.com/locate/epsl

Table 1
Trace element data for samples from Kluchevskoy volcano. Regression coefficients for trace elements versus $\delta^{18}O$ of the raw and fractionation corrected data are also shown. Strong correlations ($r > 0.6$ or $r < -0.6$) are emphasized in bold.

	KLU-01	KLU-02	KLU-03	KLU-04	KLU-05	KLU-06	KLU-07	KLU-08	KLU-09	KLU-10	KLU-11	KLU-12	KLU-13
Li	10.9	13.2	8.3	7.8	9.1	8.1	8.6	8.9	8.3	7.5	7.9	13.9	13.3
Be	0.55	0.63	0.50	0.58	0.62	0.48	0.47	0.62	0.50	0.49	0.54	0.66	0.68
Sc	33.0	29.9	35.9	35.2	35.1	34.0	36.0	30.9	35.0	35.1	36.9	21.1	27.0
V	255	259	239	249	235	245	244	246	250	256	261	260	267
Cr	256	45	424	285	241	341	500	220	343	319	320	31	6
Co	32.0	36.9	36.9	39.2	39.2	40.0	40.0	34.9	38.0	39.1	35.9	33.1	30.0
Ni	93	39	150	100	106	107	166	88	104	108	109	31	14
Cu	79	84	60	79	74	59	64	72	78	74	73	91	88
Zn	85	88	79	84	80	81	78	80	78	81	81	87	88
Ga	19.0	17.9	15.9	15.1	18.1	16.0	16.0	17.0	17.0	19.0	18.0	18.0	19.0
Rb	15.1	17.8	12.2	10.2	12.3	11.3	11.6	11.9	9.5	9.4	9.4	19.0	19.0
Sr	341	392	323	295	316	299	312	318	290	291	286	398	403
Y	18.5	21.2	14.9	19.5	17.9	15.9	15.3	18.5	17.8	18.3	19.0	22.0	21.8
Zr	87	104	81	101	99	81	77	98	87	85	85	104	105
Nb	1.46	1.75	1.15	1.70	1.67	1.17	1.31	1.78	1.43	1.46	1.39	1.99	1.92
Cs	0.43	0.47	0.42	0.36	0.46	0.28	0.39	0.39	0.33	0.31	0.32	0.51	0.48
Ba	344	396	289	224	260	283	280	260	243	224	228	435	428
La	6.09	7.55	5.41	6.12	6.69	5.03	5.31	6.72	5.54	5.32	5.36	8.43	8.20
Ce	15.1	19.3	13.6	16.3	17.1	13.0	13.1	17.5	14.3	14.2	14.6	21.1	21.3
Pr	2.49	3.16	2.17	2.62	2.77	2.14	2.13	2.83	2.38	2.34	2.46	3.39	3.54
Nd	11.9	14.9	10.4	12.4	12.7	10.2	10.3	12.9	11.2	11.4	11.6	15.8	15.6
Sm	3.35	4.07	2.94	3.54	3.41	2.91	2.99	3.50	3.07	3.21	3.25	4.14	4.11
Eu	1.06	1.26	0.90	1.07	1.04	0.94	0.93	1.07	1.01	1.02	0.97	1.27	1.29
Gd	3.32	3.75	2.89	3.52	3.35	3.01	2.87	3.35	3.18	3.20	3.20	3.77	3.76
Tb	0.54	0.62	0.45	0.57	0.54	0.48	0.46	0.56	0.53	0.55	0.56	0.63	0.65
Dy	3.42	3.82	2.87	3.66	3.27	3.07	2.91	3.46	3.36	3.42	3.42	3.84	3.82
Ho	0.71	0.77	0.61	0.79	0.69	0.64	0.59	0.71	0.68	0.70	0.70	0.82	0.81
Er	1.99	2.22	1.68	2.27	1.98	1.82	1.73	2.06	1.95	2.06	2.04	2.36	2.34
Tm	0.29	0.33	0.26	0.33	0.30	0.27	0.25	0.30	0.28	0.31	0.31	0.34	0.36
Yb	1.94	2.13	1.61	2.10	1.91	1.67	1.61	1.98	1.84	1.98	1.96	2.15	2.16
Lu	0.29	0.34	0.25	0.32	0.29	0.25	0.24	0.30	0.29	0.30	0.30	0.34	0.32
Hf	2.04	2.49	1.88	2.35	2.25	1.98	1.86	2.32	2.08	2.07	2.03	2.55	2.56
Ta	0.09	0.09	0.09	0.12	0.11	0.07	0.08	0.11	0.09	0.10	0.10	0.14	0.16
Tl	0.07	0.06	0.05	0.03	0.05	0.03	0.05	0.04	0.03	0.03	0.04	0.07	0.06
Pb	2.94	3.32	3.06	2.76	3.21	2.88	2.90	2.95	2.84	2.51	2.38	3.42	3.38
Th	0.65	0.77	0.61	0.49	0.56	0.55	0.59	0.59	0.48	0.48	0.44	0.80	0.78
U	0.42	0.49	0.41	0.33	0.40	0.40	0.40	0.38	0.34	0.32	0.31	0.49	0.46
La/Yb	3.14	3.55	3.36	2.92	3.50	3.01	3.30	3.39	3.01	2.69	2.74	3.93	3.79
Ba/Sr	1.01	1.01	0.90	0.76	0.82	0.95	0.90	0.82	0.84	0.77	0.79	1.09	1.06
U/Th	0.64	0.64	0.68	0.68	0.72	0.72	0.68	0.64	0.72	0.66	0.69	0.62	0.59

were derived from undated Holocene cinder cones and lava flows. Great care was taken to avoid any trace of alteration. Samples were large enough (1– > 10 kg) to allow separation of phenocrysts.

3. Analytical procedures

Major and trace elements (Ba, Co, Cr, Ga, Sc, Sr, Ni, V, Zn, Zr) were measured on glass fusion discs by X-ray fluorescence (XRF). From interna-

Table 1 (*continued*)

KLU-14	KLU-15	KLU-16	r	r_{70}	recom. values	JB3 ($n = 19$)	Stabwn (%)	dev. (%)	recom. values	Stabwn (%)	Stabwn (%)	dev. (%)
13.5	9.8		**0.86**	**0.89**	7.21	7.09	5.4	1.6	27.3	27.2	7.5	0.3
0.71	0.51		0.48	0.29	0.81	0.60	10.3	34.3	2.05	2.09	7.2	1.7
27.1	38.1	41.5	−0.60	−0.03	33.8	32.5		4.0	19.6	20.0		2.0
259	246	244	0.47	0.21	372	382		2.6	126	124		1.6
33	432	857	−0.52	−0.16	58	62		6.3	436	455		4.2
33.1	40.1	47.6	−0.54	−0.16	34.3	35.5		3.4	29.5	29.0		1.7
21	110	206	−0.62	0.04	36.2	33.5		8.1	130	137		4.8
83	77		0.49	0.27	194	178	8.5	9.2	29.7	28.7	4.8	3.4
89	77	56	0.47	0.24	100	104		3.4	65	62		5.2
18.0	15.0	15.2	0.24	−0.18	19.8	19.0		4.2	16.9	15.5		9.0
19.3	15.8		**0.94**	**0.95**	15.1	15.4	6.6	1.9	73	76	5.0	3.7
375	334	246	**0.85**	**0.81**	403	396		1.8	248	252		1.4
23.1	17.6		0.50	0.40	26.9	24.3	4.4	10.8	18.3	16.5	8.0	11.2
107	75	67	0.35	−0.05	98	95		3.5	116	116		0.4
2.00	1.30		0.37	0.16	2.47	2.04	8.6	21.3	9.47	9.29	10.2	1.9
0.58	0.44		**0.72**	**0.63**	0.94	0.93	5.6	1.5	4.63	5.01	7.9	7.5
403	308	229	**0.92**	**0.93**	245	241		1.7	321	319		0.8
8.42	6.80		**0.71**	**0.70**	8.81	8.40	3.3	4.9	15.8	16.2	6.6	2.7
21.5	17.0		**0.65**	**0.63**	21.5	21.3	3.7	0.9	32.7	34.3	4.9	4.6
3.61	2.71		**0.64**	**0.63**	3.26	3.42	3.4	4.7	3.84	4.14	2.8	7.4
16.7	12.3		**0.64**	**0.65**	15.6	16.4	3.6	4.9	13.9	15.7	2.5	11.5
4.27	3.36		**0.64**	**0.65**	4.27	4.56	2.9	6.3	3.11	3.39	3.7	8.2
1.33	1.02		**0.66**	**0.72**	1.32	1.32	4.2	0.3	0.93	0.92	3.4	1.2
3.88	3.04		0.50	0.36	4.67	4.46	3.7	4.8	3.06	3.06	4.8	0.1
0.64	0.51		0.44	0.24	0.73	0.73	3.2	0.6	0.44	0.48	5.4	7.5
4.04	3.05		0.39	0.12	4.54	4.38	2.7	3.7	2.80	2.78	5.2	0.8
0.83	0.66		0.43	0.21	0.80	0.89	2.8	10.3	0.50	0.60	4.0	16.2
2.38	1.84		0.35	0.05	2.49	2.57	3.2	3.0	1.48	1.70	3.3	13.2
0.34	0.28		0.38	0.10	0.42	0.38	3.0	11.5	0.28	0.25	3.6	11.8
2.26	1.69		0.30	−0.04	2.55	2.42	2.8	5.5	1.62	1.60	3.6	1.1
0.33	0.26		0.23	−0.16	0.39	0.36	2.6	8.4	0.27	0.24	3.8	10.5
2.57	1.89		0.41	0.15	2.67	2.61	5.6	2.4	2.86	2.95	6.3	3.1
0.14	0.09		0.34	0.19	0.150	0.157	60.9	4.4	0.80	0.72	24.6	10.5
0.05	0.02		**0.63**	0.52	0.048	0.047	22.6	2.9	0.32	0.33	11.4	3.8
3.66	2.86		**0.72**	0.43	5.58	5.05	4.8	10.6	19.2	19.2	9.4	0.0
0.79	0.71		**0.94**	**0.87**	1.27	1.32	9.3	4.1	5.03	4.84	6.8	4.0
0.49	0.39		**0.86**	**0.70**	0.48	0.47	4.4	1.8	2.21	2.19	5.8	0.9
3.73	4.03		**0.75**	**0.71**								
1.07	0.92	0.93	**0.90**	**0.89**								
0.62	0.55		**−0.74**	**−0.74**								

tional standards (JA2, JB3) and duplicated measurements the precision (relative 2σ error) for major elements is estimated at $< 1\%$ (except FeO and $Na_2O = 2\%$) and $< 5\%$ for trace elements with abundances > 20–30 ppm. Other trace elements were determined by ICPMS. The international standards JB3 ($n = 19$) and JA2 ($n = 8$) were measured as unknowns in the experiments. From this the 2σ error of the method is estimated to be $< 20\%$ for Nb and Ta, $< 10\%$ for Be, Cs, Cu, Hf,

Li, Y, Pb, Rb, Tl, Th and U and ∼5% for the rare earth elements (REE). Water contents were determined by Karl Fischer titration (2σ around 10%).

Oxygen isotope ratios of olivine were measured at the Geophysical Laboratory, Carnegie Institution using a Synrad Series 48 CO_2 laser. The technique is similar to that in [14]. Oxygen, however, was not converted to CO_2 after reaction of samples with BrF_5, but frozen on a molecular sieve. The isotopic composition of oxygen is determined on masses 32, 33, and 34 on a Finnigan MAT-252 mass spectrometer. The oxygen standard gas was calibrated to the SMOW scale using NBS-28 ($\delta^{18}O = 9.60‰$). Analyses of NBS-28 were performed by rapid heating with a defocused laser beam [15], in order to avoid grain size effects. Daily variations were corrected by an in-house olivine standard ($\delta^{18}O = 5.2‰$). The external error of this method is estimated to be better than $\pm 0.2‰$ based on five analyses of NBS-28 ($9.57 \pm 0.18‰$, 2σ), a mean of $5.85 \pm 0.06‰$ for two analyses of UWG-2, a garnet standard used at the University of Wisconsin, and an average reproducibility (2σ) better than $\pm 0.2‰$ for multiple runs. Single 1–2 mm large Ca-rich pyroxene crystals were analyzed using an ultraviolet (UV) ArF laser in Göttingen and a Finnigan MAT-251. On average the reproducibility of pyroxene analyses is less than analyses of olivines. This may be due to inclusions of matrix minerals and surface contamination rather than true heterogeneity. Pyroxene data have been corrected using the same olivine standard as described above, ensuring accurate and comparable calibration to the SMOW scale.

The isotope ratios of Sr and Nd on corresponding whole rocks were measured at a Finnigan MAT262-RPQIIplus in Göttingen. The Sr and Nd isotope ratios were corrected for mass fractionation to $^{86}Sr/^{88}Sr = 0.1194$ and $^{144}Nd/^{146}Nd = 0.7219$ and referenced to NBS987 (0.710245) and La Jolla (0.511847). Measured values of these standards over the period of the study were 0.710262 ± 24 (9 analyses) and 0.511847 ± 20 (11 analyses). Lead isotopes were corrected to NBS981 [16]. Thirteen analyses of this standard gave a mean of $^{206}Pb/^{204}Pb = 16.90 \pm 0.01$, $^{206}Pb/$

$^{204}Pb = 15.44 \pm 0.02$ and $^{206}Pb/^{204}Pb = 37.53 \pm 0.05$. Blanks for Sr, Nd and Pb are < 1 ng, < 0.03 ng and < 0.5 ng, respectively. From continuous measurement of standards and repeated measurements of samples, total errors (2σ) less than 0.004% for Sr and Nd, and less than 0.1% for Pb isotopes were determined.

4. Analytical results

4.1. Major and trace elements

Our samples represent HMB and HAB with SiO_2 ranging from 52 to 54 wt% and MgO from 4.6 to 11.7 wt% (Fig. 2, **EPSL Online Background Dataset**, Table 1, see footnote 2). The trace element pattern is typical for Quaternary volcanic rocks of Kamchatka and for island arcs in general, i.e. with relative depletions in HFSE and enrichment in LILE (Table 1, Fig. 3). From the N-MORB-normalized Nb_N/Yb_N range of 0.8–1.0 we argue for a mantle source similar to that of the N-MORB. Low HREE concentrations can be explained by relatively high melting degrees ($\sim 20\%$). Sr isotope ratios of Kluchevskoy volcano have a narrow range from 0.70351 to 0.70366 and are slightly enriched compared to other Quaternary lavas from Kamchatka (Table 2, Fig. 4).
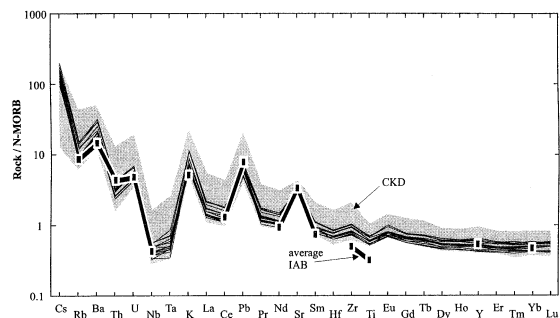

Fig. 3. N-MORB-normalized trace element pattern of Kluchevskoy volcano/Kamchatka (thin lines). Note the typical arc signature with strong enrichment in LILE and depletion in HFSE, typical for rocks from Kamchatka (own unpublished data of the CKD are used as reference) and average arc basalts in general [38]. N-MORB composition and the order of incompatible elements (enlarged by Cs and all REE) after [39].

Table 2

Mineral laser oxygen data (in ‰ relative to SMOW) and radiogenic isotope ratios for corresponding whole rocks from Kluchev-skoy volcano. Melt oxygen isotope ratios ($\delta^{18}O$) were calculated from the mean of olivine data ($\delta^{18}O_{ol}$), assuming an olivine melt fractionation of -0.4‰

Sample	Rock type	Phenocrysts	$\delta^{18}O_{ol}$	$\delta^{18}O_{cpx}$	$\delta^{18}O$	$^{87}Sr/^{86}Sr$	$^{143}Nd/^{144}Nd$	$^{206}Pb/^{204}Pb$	$^{207}Pb/^{204}Pb$	$^{208}Pb/^{204}Pb$
KLU-01	HMB	plag, cpx, ol	6.90 6.90 6.82	6.51 7.40 7.43	7.27	0.70356	0.51309	18.31	15.50	37.97
KLU-03	HMB	ol, cpx	6.40 6.36 6.32 6.50	6.68 6.45	6.80	0.70357	0.51310	18.28	15.50	37.97
KLU-04	HMB	plag, cpx, ol	5.97 5.86	6.21 6.43	6.32	0.70353	0.51307	18.28	15.50	37.97
KLU-05	HMB	plag, cpx, ol	5.93 5.84		6.29					
KLU-06	HMB	ol, cpx	6.36 6.43	6.80 6.44	6.80	0.70355	0.51309			
KLU-07	HMB	ol, cpx	6.28 6.19	7.15 7.07 6.77	6.64	0.70355	0.51307	18.30	15.50	37.97
KLU-08	HMB	plag, cpx, ol	6.00 6.01	5.73 6.49	6.41	0.70352	0.51308	18.30	15.52	38.01
KLU-09	HMB	plag, cpx, ol	5.82 5.83	6.40 6.43 6.27	6.23	0.70351	0.51311			
KLU-10	HMB	plag, cpx, ol	5.85 5.78	6.57 6.46	6.22	0.70352	0.51311	18.29	15.51	38.00
KLU-11	HMB	plag, ol, cpx	5.84 5.82	6.28 6.56	6.23	0.70353	0.51310	18.29	15.50	37.97
KLU-15	HMB	ol, cpx	6.95 6.97 6.89	7.26 6.72	7.34	0.70355	0.51312	18.30	15.49	37.94
KLU-16	HMB	ol, cpx	5.97 6.09		6.43					
KLU-02	HAB	plag (ol, cpx)	7.07 6.99	7.15 7.36	7.43					
KLU-12	HAB	plag (ol, cpx)	6.89	7.66 7.22 7.21	7.29	0.70366	0.51309	18.30	15.51	38.00
KLU-13	HAB	plag (ol, cpx)	7.13		7.53	0.70366	0.51309			
KLU-14	HAB	plag (ol, cpx)	7.05 7.09	7.63 7.56 7.73	7.47	0.70362	0.51309			

HAB are more radiogenic in Sr isotopes compared to HMB. Pb and Nd isotopic ratios are MORB-like (Fig. 4). These results are consistent with [17].

Major and trace element trends can be approximated by olivine and clinopyroxene (1:2 mass ra-tio) fractionation from a parent composition such as sample KLU-16 (Fig. 2). Compared to HMBs, the HABs form a tight compositional group, probably caused by limited sample numbers and eruptions from the same magma batch close in time (1951, 1953, and 1966). Combining our
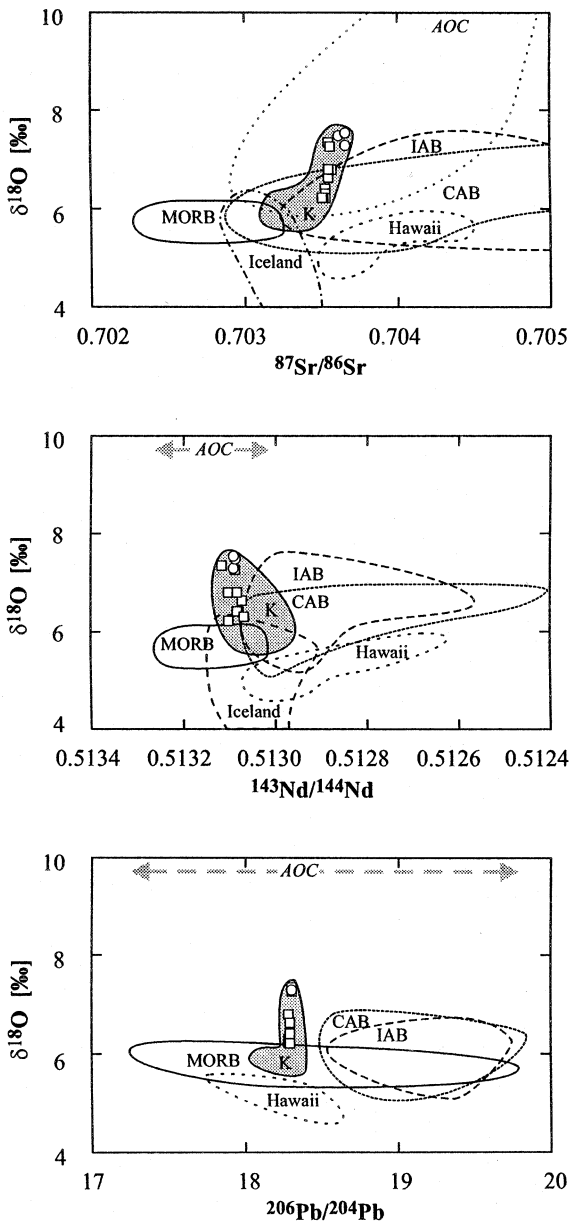
4.2. Oxygen isotopes

The oxygen isotope ratios of single olivines from different rocks vary from 5.8‰ to 7.1‰ (Table 2). Replicate samples are reproducible to within 0.2‰. Results for pyroxene give a range from 5.7 to 7.7‰. Pyroxene is on average 0.4‰ heavier than olivine from the same rock, consistent with cpx-ol fractionation [19]. Melt values are calculated from the mean $\delta^{18}O$ of olivine, using olivine melt fractionation of −0.4‰ at 1100–1200°C [19]. The resulting range of 6.2–7.5‰ is clearly larger and values are distinctly higher than for typical mantle-derived melts (e.g., [4]).

Fig. 5. Correlations of $\delta^{18}O$ with fluid-mobile elements like K (shown as oxide), Ba, Rb and Pb. Measured data: open symbols; fractionation-corrected values: closed symbols. Analytical error, regression lines and regression coefficients are shown for the crystal fractionation-corrected data. Strong positive correlations for K, Ba and Rb and only a weak positive trend for Pb with $\delta^{18}O$ are notable.

own with published data [10,11,18] the HABs show some scatter in major elements, LILE, K_2O/Na_2O, Ba/Zr, La/Yb. This scatter and lack of correlation between LILE and HFSE do not allow for a single parental magma. Therefore we have to assume that processes additional to crystallization are required to explain the major and trace elements, and isotopic data.

Having established this unusual range in O isotope composition, we will now explore correlations between $\delta^{18}O$ and other geochemical and isotopic parameters (Figs. 4–7) in order to understand the origin of these variations.

A steep trend is observed between O isotopes and $^{87}Sr/^{86}Sr$ (Fig. 4). Historic rocks tend to have higher $\delta^{18}O$ and Sr isotopic ratios compared to Holocene samples. There are also positive correlations between $\delta^{18}O$ and some trace elements (Cs, Li, Sr, Ba, Rb, Pb, Th, U, LREE) and K, i.e. elements which are known to be enriched in slab-derived fluids (named 'fluid-mobile' elements hereafter). Strong positive correlations are also observed between O isotopic ratios and oxide or elemental ratios such as K_2O/Na_2O, Ba/Zr and La/Yb (Fig. 7). A negative correlation of $\delta^{18}O$ was found with U/Th.

Some of the elemental variability is due to crystal fractionation. To correct for this, all concentrations were recalculated to Mg#70 by adding olivine and clinopyroxene in proportions of 1:2 (Table 1 and **EPSL Online Background Dataset**, Table 1, see footnote 2, Figs. 2, 5 and 6; filled symbols). Mineral major element compositions were derived from the microprobe data of [10], trace elements were calculated using melt/liquid distribution coefficients in [20]. This approach
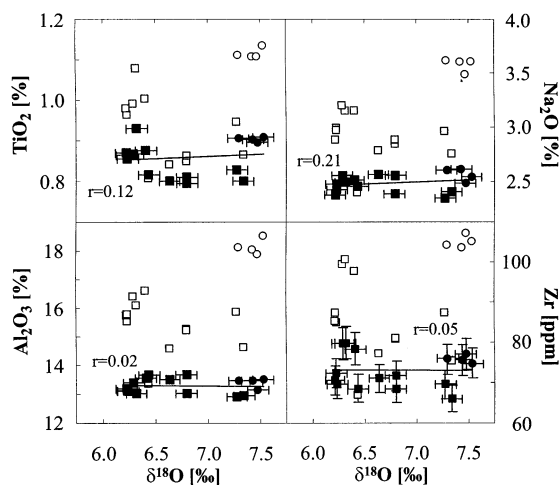

Fig. 7. Correlations of $\delta^{18}O$ with trace element ratios. The analytical error (2σ), regression lines and regression coefficients are also shown. The ratios were calculated from the original measured data, because fractionation should have no influence on incompatible element ratios.

provides an effective fractionation correction for all incompatible trace elements and some major elements (K, Ti, P and Al). A maximum of 30% fractionation is calculated for most evolved HABs. Corrected fluid-mobile element concentrations still strongly correlate with $\delta^{18}O$. Interestingly, weak correlations between those elements which are immobile in fluids but can be transported in melts like Al and HFSE (named 'melt-mobile' elements hereafter) disappear after the fractionation correction.

5. Discussion

Fractionation of olivine will increase the $\delta^{18}O$ of the melt by less than 0.1‰ and pyroxenes do not have any detectable effect [19]. Fractionation of magnetite is insignificant relative to other phases because depletion in FeO or TiO_2 is not observed. Separation of other minerals such as plagioclase or quartz would even lower $\delta^{18}O$ in the magma. It is obvious that separation of mafic minerals is not responsible for the increased oxygen isotope ratios in the Kluchevskoy lavas.

Remaining options to explain a substantial change in oxygen isotopes in Kluchevskoy mag-

Fig. 6. Plot of $\delta^{18}O$ versus melt mobile elements Ti, Na, Al (shown as oxides), and Zr. Symbols as in Fig. 5. The analytical error, regression lines and regression coefficients are shown for the fractionation-corrected data. There are no correlations of this group of elements with $\delta^{18}O$.
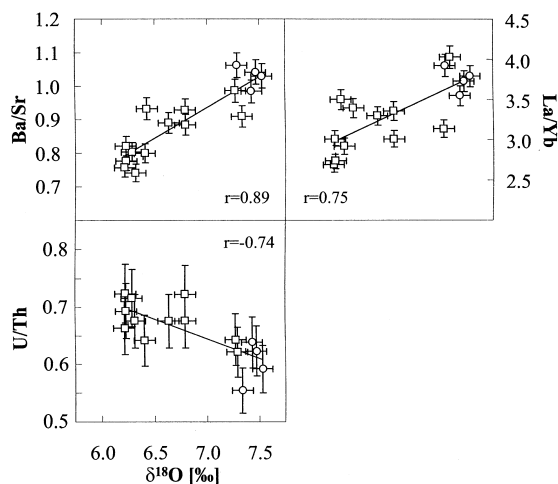
mas are: (1) crustal assimilation; (2) source contamination by subducted sediments; or (3) fluids from the altered oceanic crust in the mantle source. These possibilities are evaluated in the following sections.

5.1. Crustal assimilation
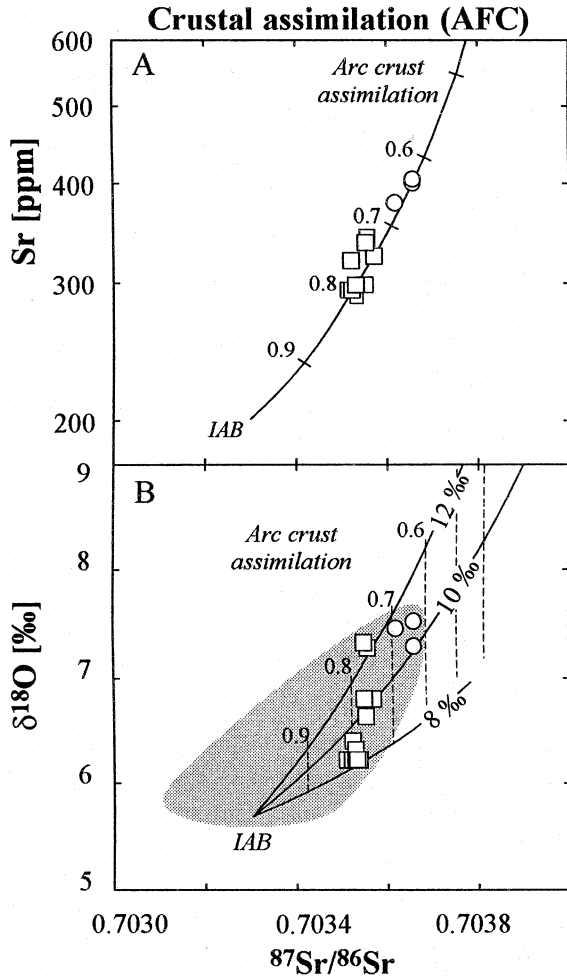
Assimilation of old crust is known to cause ^{18}O

Fig. 8. AFC model for Sr, $^{87}Sr/^{86}Sr$ and $\delta^{18}O$, calculated for assimilation of primitive island arc basalt magmas by hydrated ^{18}O-enriched island arc crust (Table 3) with variable $\delta^{18}O$ (8, 10, 12‰) but similar Sr and $^{87}Sr/^{86}Sr$ composition. Tick marks express F, the remaining melt fraction. Plotted Sr data are measured uncorrected values. The gray field represents the data for basalts from all Kamchatka (unpublished data of the authors).
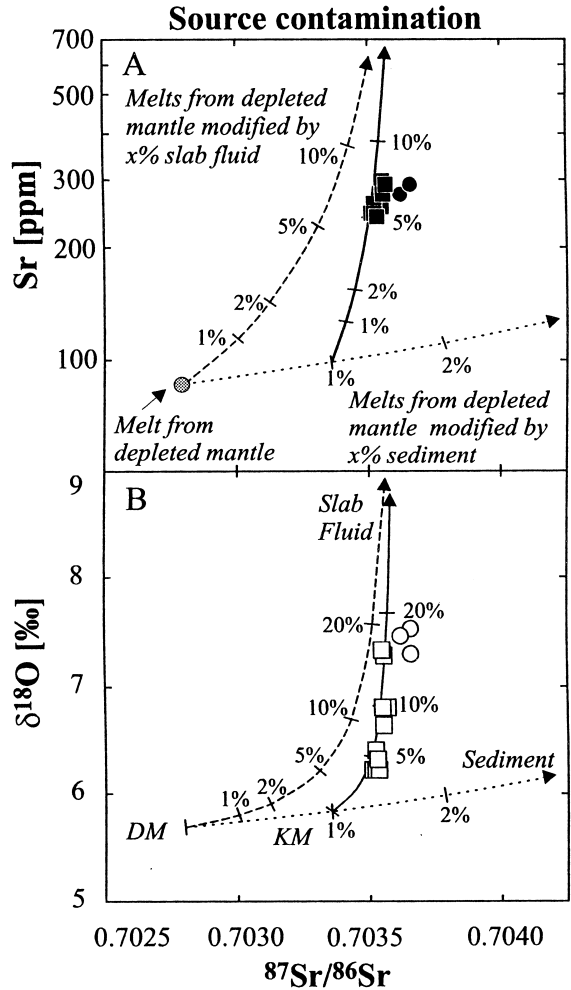

Fig. 9. Source contamination model, showing melt compositions derived from a mantle source modified by variable additions of sediment and/or slab fluid (mixing endmembers derived from Table 3) shown in (A) $^{87}Sr/^{86}Sr$-Sr and (B) $^{87}Sr/^{86}Sr$–^{18}O space. Lines in A and B represent melts, derived from 10% melting of such contaminated mantle, the degree of source contamination is shown by tick marks. Fractionation-corrected data are plotted in A, to approximate primary melt composition.

enrichment of volcanic rocks in continental arcs (e.g., [4]). Even OIBs erupting through thin oceanic crust can be strongly contaminated by altered basalts [6]. Therefore assimilation of ^{18}O-enriched crust needs to be tested to explain the O isotopic characteristics of Kluchevskoy lavas.

The crust below the CKD consists of Cretaceous to Tertiary accreted arc and oceanic mate-

Table 3
Parameters used in the mixing and AFC models

	Sediment[a]	DM[b]	KM[c]	IAB[d]	Slab fluid[e]	Arc crust[f]
$\delta^{18}O$ (‰)	20	5.7	5.8	5.8	12	8; 10; 12
O (%)	50	50	50	50	85	50
$^{87}Sr/^{86}Sr$	0.707	0.7028	0.7033	0.7033	0.7036	0.7046
Sr (ppm)	250	16.6	19	200	550	200

[a]Sediment composition assumed to be in equilibrium with Cretaceous sea water, Sr after [24].
[b]Depleted mantle (DM): $\delta^{18}O$ and $^{87}Sr/^{86}Sr$ after Ito et al. (1987), Sr after [28].
[c]Mantle source below Kluchevskoy volcano (KM) calculated as 99% DM+1% sediment.
[d]Primitive island arc basalt (IAB) melt used in the AFC modeling, Sr were empirically derived to approximate the observed trends.
[e]Slab fluid derived from altered oceanic crust [25,26].
[f]The $\delta^{18}O$ value for arc crust corresponds to AOC, $^{87}Sr/^{86}Sr$ and Sr were empirically derived to approximate the observed trends.

rial [12]. Such young volcanic rocks or volcani-clastic sediments can be close to mantle values in Pb and Nd isotopes. Sr and oxygen isotopic compositions may be more variable, because of low T exchange with seawater. From dacitic rocks of the Bonin Islands $\delta^{18}O$ values up to +15‰ are known, whereas pyroxene phenocrysts of the same rocks give mantle values [22]. Obviously, arc basalts and OIBs erupting into a submarine environment can become ^{18}O-enriched by seawater alteration.

In Fig. 8 we try to model the apparent correlation between $\delta^{18}O$ and Sr by AFC (Table 4). The relative rate of assimilation of arc crust to the rate

Table 4
Rock and fluid compositions used in the slab–wedge interaction model (all concentrations in ppm). Differences between the compositions of the calculated fluids and those from the literature data [26,40] are caused by slightly different input parameters in the modeling

	EM[a]	Slab[b]	Slab fluid (SF)[c]		Wedge fluid (WF)[d]		SF/WF	SF/EM
			[40]	[26]	[40]	[26]		
Rb	0.38	9.58	71		1.09		65	186
Ba	10.47	22.6		2210		173	13	211
Th	0.036	0.7		1.69		0.33	5.1	47
U	0.017	0.3		0.59		0.33	1.8	36
Pb	0.090	0.3		15		4.80	3.1	168
Sr	17.8	115	180	575	47	100	4–6	32
Nb	0.36	1.22	0.04	0.36	0.23	2.55	0.1–0.2	0.1–1.0
Zr	8.62	66.5	1.70		22		0.1	0.2
La	0.41	1.84	0.84		0.81		1.0	2.1
Sm	0.40	2.5	0.01		0.04		0.3	0.03
Tm	0.30	0.43	0.001		0.005		0.3	0.005
Y	22.6	26.9	0.03		0.41		0.1	0.001
U/Th	0.46	0.43		0.35		0.99	0.4	0.8
La/Tm	1.36	4.28	612		170		3.6	450
Ba/Sr	0.59	0.20		3.85		1.73	2.2	6.6

[a]Enriched mantle calculated from depleted mantle [28], contaminated by 0.5% sediment [24].
[b]Slab composition (upper part of altered oceanic crust) after [25], Pb after [38].
[c]Calculated fluid (1%) in equilibrium with the slab (59:40:1 by mass garnet:clinopyroxene:rutile), using $D_{mineral/fluid}$ values of [40] and [26].
[d]Calculated fluid (1%) composition in equilibrium with the EM (60:30:10 by mass olivine:orthopyroxene:amphibole), using $D_{mineral/fluid}$ values of [40] and [26].

of crystallization (*r*) is taken at 0.5. A low Sr content of only 200 ppm for the primitive magma (IAB in Fig. 8) is consistent with the lowest Sr concentrations in most mafic Kamchatka lavas (215 ppm, Bakening volcano, Dorendorf et al., submitted). Given the model parameters as in Table 3, the AFC model can, in principle, explain the data only if the Sr isotopic composition of the parent is significantly more radiogenic than a depleted MORB source (Figs. 8 and 9).

To produce the most ^{18}O-enriched HAB from a mantle-derived magma with ^{18}O = 5.7‰ by AFC, the magmas need to be extensively fractionated, between $F = 0.9$ and $F = 0.65$ for the different AFC curves. This translates into a proportion of 10–23% assimilated mafic crust. At this proportion, the assimilant forms up to 45% of the resulting magma. Even the most primitive sample (KLU-16) with $\delta^{18}O = 6.4‰$ would need $> 20\%$ fractionation and $> 10\%$ assimilation, which is not consistent with its primitive Mg# number of 71. An AFC process should also strongly increase the contents of SiO_2 and all incompatible trace elements. In addition, from thermal balance arguments, it is impossible for a basaltic magma to assimilate large volumes of basaltic wall rock. Similar arguments argue against assimilation of accreted oceanic sediments. We conclude that, although fractional crystallization has affected the bulk rock composition, assimilation of crustal rocks cannot explain the observed high oxygen isotope ratios and Sr–O isotope trend.

5.2. Source contamination by sediments

It is well established by geochemical and isotopic composition in arc rocks that sediments contribute to arc volcanism (e.g., [1]). Sediments also have the potential to enrich the mantle in $\delta^{18}O$. Northwest Pacific sediments are rich in siliceous ooze and reach $\delta^{18}O$ values of up to 30‰ [23]. At subduction, fluids or melts derived from such sediments might introduce an ^{18}O-rich component into the mantle. In order to test the role of such sediment component, we calculated simple binary mixing between oceanic sediments (^{87}Sr/^{86}Sr = 0.707 and $\delta^{18}O = 20‰$) and a depleted MORB mantle [7]. Sediment Sr concentrations

are from [24], the ^{87}Sr/^{86}Sr and δ^{18}O are assumed to be in equilibrium with Cretaceous seawater.

The model (Fig. 9) calculates Sr, ^{87}Sr/^{86}Sr, and δ^{18}O compositions in melts from a mantle source (DM) that has been modified by the addition of subducted sediment. A minor sediment contribution to the mantle source would drastically change Sr, Nd, and Pb isotope ratios but not significantly change δ^{18}O and Sr contents in resulting melts (almost horizontal dotted lines in Fig. 9). Involving melts or fluids from sediments would give similar results. A sedimentary component to explain the ^{18}O enrichment in Kluchevskoy magmas is thus ruled out.

5.3. Source contamination by fluids from the altered oceanic crust

The upper oceanic crust is ^{18}O-enriched by hydrothermal alteration and exchange with seawater (e.g., [25]). Changes in Nd and Pb isotopes in altered MORB are small due to low Nd and Pb abundances in seawater. The upper oceanic crust is further characterized by ^{87}Sr enrichment, which strongly correlates with δ^{18}O [25]. From these data, a maximum of $\delta^{18}O = 12‰$ is assumed for the upper (low T) altered oceanic crust, subducted below Kluchevskoy. Similar values can be inferred for subducted seamount material. Aqueous fluids released by the breakdown of hydrous minerals have been shown experimentally (e.g., [26,27]) to be enriched in alkalis, alkaline earths, U, Th, and Pb but to be essentially free of HFSE and HREE.

We calculated melt compositions from a mantle source that is variably enriched in a sediment component (no sediment = DM; 1% sediment = KM, see discussion above) and a variable fluid component with ^{18}O = 12‰ (1, 2, 5, 10, 20%, dashed and solid lines in Fig. 9). For parameters used see Tables 3 and 4.

A large contrast in Sr concentration between slab-derived fluids (550 ppm Sr [26]) and depleted mantle (16.6 ppm Sr [28]) results in a strong leverage of the fluid on the mantle Sr isotope composition for low fluid proportions (up to 5%). Beyond 5% fluid addition, this process will cause a steep trend between Sr and O isotopes because

of the relatively unradiogenic Sr isotope composition of the fluid. The calculated trends fall close to the observed compositions, however the amount of fluid in the source (5–20 wt%) is rather high. Such large amounts of hydrous fluid would cause extensive and unrealistically high degrees of melting [2]. It was argued for Kamchatka that the ^{18}O-rich component is a hydrous melt rather than a hydrous fluid [8]. However, hydrous melts are quite different in trace elements to hydrous fluids, particularly in their high HFSE [26]. From trace element patterns of Kluchevskoy samples and the correlation between $\delta^{18}O$ and trace elements (or lack thereof for HFSE) a role for a hydrous melt component is ruled out.

Time elapsed between fluid enrichment in the arc magma source, melting and eruption is in the order of 30 000– >150 000 years [29,30]. Therefore in our model, the increase of U/Th, connected with the depletion in ^{18}O, should be expressed in a measurable U–Th isotope disequilibrium. However, in a preliminary study no [238]U/[230]Th disequilibrium could be found in Kluchevskoy samples which argues against a recent (< 300 000 years) fluid-induced melting event.

6. A $\delta^{18}O$-enriched mantle source?

In the previous section we calculated a mixture between the mantle and a slab-derived fluid, with the result of unrealistically high amounts of fluid in the magma source. However, if we allow for time, the amount of infiltrating fluid at any given stage can be much less than that estimate for the bulk rock/water ratio. In the next sections we develop the following model:

1. Small amounts of hydrous ^{18}O-enriched fluid liberated from the slab migrate into the overlying non-convecting cold lithosphere of the mantle wedge. Such small volumes of fluid can (over time of some m.y.) produce a mantle that has exchanged at a high fluid/rock ratio. A proportion of 20% fluid (see above) will then be possible without extensive melting.
2. The fluid forms hydrous minerals in the mantle. Its type and quantity depend on the P–T conditions in the mantle wedge and the chemical composition (i.e. availability of K, Na, Al) from the mantle and fluid. Only a small amount of fluid will be instantly fixed in hydrous phases, the remaining part will migrate further into the mantle until it is completely reacted.
3. Equilibration with mantle mineralogy and the newly formed hydrous minerals will result in a concentration profile of [18]O and certain trace elements from the slab into the mantle. In an extreme case, the mantle close to the slab is completely equilibrated with the slab fluid and the fluid far away from the slab is completely equilibrated with the mantle minerals. The composition of the mantle and the two fluids can be modeled by percolation [31] or zone refining [3]. To simplify the model, we only discuss the endmember compositions. Co-variation of trace elements and radiogenic isotopes with $\delta^{18}O$ is then produced by mixing these endmembers.
4. Such metasomatized mantle becomes involved in arc magmatism due to intra-arc rifting of the CKD. Mixing of the differently metasomatized mantle regions creates the observed geochemical and isotopic correlations with $\delta^{18}O$.

This model represents a chromatographic process which implies the possibility of different length scales for the profiles of different elements. However, we have no independent constraint as to where melting takes place within the spectrum of percolation-modified compositions. To simplify the model, we only discuss the endmember compositions and co-variations of trace elements and radiogenic isotopes with $\delta^{18}O$ are then assumed to be produced by mixing these endmembers.

6.1. Mantle composition

Nb_N/Yb_N of Kluchevskoy samples shows that their source was similar to or even more depleted than the MORB source (Fig. 3). From the trend in Sr and O isotopes, it is shown that this source was contaminated by some limited amounts of sediment. We calculated the mantle wedge source

below Kamchatka (KM) as a mixture of depleted mantle and 1% maximum of sediment (Table 4).

6.2. Slab fluid composition

A critical parameter in our model is the composition of the two endmember fluids. The infiltrating slab fluid depends on pressure, temperature, and mineralogical composition of the slab. The P–T conditions in the uppermost part of the slab in the region underlying the lithospheric mantle can be estimated using the model of [32]. The situation for Kamchatka is similar to the Aleutians, i.e. fast subduction of an old slab, which results in a relatively cold P–T path (T = 200–600°C at 1–3 GPa). At these conditions, the slab fluid should be a hydrous fluid. Experiments on trace elements in hydrous fluids were performed exclusively at temperatures exceeding 900°C. Fluid/mineral partition data are thus only available for phases in the deeper part of the slab, such as garnet, clinopyroxene, amphibole, rutile, orthopyroxene and olivine [3,26,27]. The fluid/mineral partition behavior for other phases like apatite, lawsonite, chlorite, chloritoid, epidote, zoisite–clinozoisite, phengite and serpentine, likely to be residual in shallower regions, is unknown. However, even minor amounts of these phases may strongly influence trace elements in the fluid. For example K, Rb, Ba and Cs are carried essentially by phengite [33], Y and REE by lawsonite and apatite [34]. A more reliable estimate of the fluid composition is be derived from studies of high-pressure metamorphic terranes [33,35]. From these studies it is concluded that slab fluids released at shallow pressures will also be enriched in LILE and LREE but poor in HREE and HFSE and thus be similar to the deep-derived fluids.

The slab fluid composition was then calculated from $D_{\mathrm{mineral/fluid}}$ data for 2–3 GPa and 900–1100°C of [3,26] assuming 1% fluid dehydration from an eclogite composed of 40% clinopyroxene, 59% garnet and 1% rutile. These assumptions are identical to those of [26]. We use the estimates of [25,36] for elemental compositions of altered MORB. The $\delta^{18}O$ of the altered MORB is taken

as +12‰, consistent with $\delta^{18}O$ in water-rich melt inclusions from mantle xenoliths [37].

6.3. Wedge fluid composition

Fluids derived from the slab will percolate into the mantle wedge and react with mantle minerals to form hydrous phases such as serpentine, chlorite, talc, amphibole or phlogopite depending on P and T. If no further mantle minerals can be formed, because of a depletion in Na, K, and Al, the remaining fluid will migrate in unreacted mantle regions. The trace element content of this fluid migrating through the mantle depends on its initial composition and extent of exchange with mantle minerals. The mantle-equilibrated fluid composition can then be calculated from partition coefficients between the mantle minerals and the fluid [3,26]. Missing data for $D_{\mathrm{mineral/fluid}}$ in amphibole and orthopyroxene were calculated from $D_{\mathrm{cpx/fluid}}$ data in [3,26] and combined with $D_{\mathrm{cpx/melt}}$, $D_{\mathrm{amph/melt}}$ and $D_{\mathrm{opx/melt}}$ from [20]. The model mantle contains 60% olivine, 30% orthopyroxene, and 10% amphibole; its composition is shown in Table 4. The limited availability of $D_{\mathrm{mineral/fluid}}$ restricts the considered elements to Rb, Ba, Th, U, Pb, Sr, Nb, Zr, Y, La, Sm and Tm (missing D_{Tm} calculated from $D_{\mathrm{Tm}} = (D_{\mathrm{Er}}+D_{\mathrm{Yb}})/2$).

6.4. Elemental variations with $\delta^{18}O$

Combining the three endmembers outlined above, we can now test the model in explaining the observed elemental and isotopic correlations.

The slab and wedge fluid (Table 4) interacts with and creates two different mantle compositions that may be taken as endmember magma sources. The degree of mantle enrichment or depletion of a fluid-mobile element by the migrating fluid is described by the ratio between the concentration of that element in the slab-equilibrated fluid (C_{SF}) and the concentration in the wedge-equilibrated fluid (C_{WF}). If $C_{\mathrm{SF}} > C_{\mathrm{WF}}$, the trace element content will decrease with distance to the slab. These elements should positively correlate with $\delta^{18}O$. We can thus predict the direction of

elemental variations based on this model for different elements.

6.5. Fluid-mobile elements

From $C_{SF} > C_{WF}$ (Table 4) enrichments can be predicted for Ba, Sr, Rb, La, Th, U and Pb in the slab fluid-modified mantle which (at 5–20% fluid interaction) also has the appropriate ^{18}O-enriched isotope composition. Mixing magmas from these sources (or mixing the distinct mantle domains before melting) will cause the observed positive correlations between δ^{18}O and slab fluid-enriched elements. Our model predicts that Rb and Ba, which have the highest C_{SF}/C_{WF}, should be particularly well correlated with δ^{18}O. This is in fact what we see (Table 1, Fig. 5). Residual phlogopite in the wedge would even increase C_{SF}/C_{WF} for Rb and Ba and retain these elements from the wedge fluid. This is supported by positive correlations of ratios of K, Ba and Rb with all other fluid-mobile elements versus δ^{18}O (shown by Ba/Sr in Fig. 7).

All mantle minerals including amphibole have very low $D_{mineral/fluid}$ values for Pb. Therefore the reacting fluid remains undepleted in Pb ($C_{SF} \sim C_{WF}$), which explains that Pb only weakly correlates with δ^{18}O.

U/Th of the fluid migrating though the mantle is increased because Th is more compatible in clinopyroxene than U [26]. Garnet would cause the opposite effect, which suggests that garnet is not a stable phase in the mantle source. The relatively high U/Th for Kluchevskoy compared to other volcanoes of Kamchatka may be an indication that melts derived from a strongly metasomatized mantle dominate, as is supported by the general correlation between U/Th and Ba/Nb in Kamchatka lavas (unpublished data).

6.6. Melt-mobile elements

The HFSE (Nb, Zr), Y and all REE except La have $C_{SF} < C_{WF}$ resulting in their relative enrichment in the wedge fluid and a depletion in these elements in the reacted mantle. However, the predicted difference is small. Garnet, which has a major influence on the LREE/HREE, is present in the slab but is rare or absent in the mantle

source. This causes the four times higher La/Tm in the calculated slab fluid compared to the wedge fluid and corresponds to the observed positive correlation of LREE/HREE with δ^{18}O (Fig. 7) and a positive correlation between La/Yb and Nb/Yb.

6.7. Sr, Pb and Nd isotopes

Sr and Pb contents are low in the mantle but have high concentrations in both calculated fluids. Therefore the Sr and Pb isotope ratios of the metasomatized mantle will be strongly controlled by the isotope composition of the slab. ^{87}Sr/^{86}Sr and Pb isotopic ratios show almost no co-variations with δ^{18}O in Kluchevskoy samples. Interestingly, the field for Pb isotopes from Kluchevskoy and for Kamchatka as a whole overlaps with the fields of the Hawaii plume (Fig. 4). If we assume that the Hawaiian plume component has not significantly changed isotopically in Pb over the last 100 Ma, we can explain the Pb isotopic ratios in the Kluchevskoy rocks to be largely derived from fluids of this altered plume material.

Nd will behave similarly to Sm, which has low concentrations in the slab fluid compared to the mantle. Therefore the Nd isotope ratio will be defined almost entirely by the wedge and a correlation with δ^{18}O is not expected. This is observed in our data.

6.8. Special conditions for Kluchevskoy?

Several specific plate tectonic conditions exist for Kluchevskoy volcano, which may be the reason that the process of lithospheric ^{18}O enrichment by slab fluids can be detected here:

1. Slab dehydration at shallow levels prior to melting or ^{18}O-enriched fluids in subducted oceanic crust are not unique to Kamchatka. A special feature of subduction below the Kluchevskaya Group, however, is the subduction of the Emperor seamount chain, one of the largest of its kind on the globe. This chain is composed essentially of low T hydrothermal altered pillow lavas and volcaniclastics. Fast subduction of the relatively old and cold Pacif-
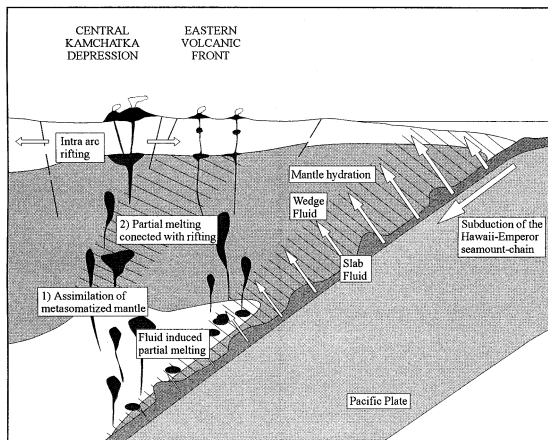
Fig. 10. Model of sub-arc lithospheric metasomatism which can explain the strong [18]O and fluid compatible element enrichment in primitive basaltic andesites of Kluchevskoy volcano. Special features of the subducting slab (old low T altered ocean island chain, fast subduction) led to an influx of large amounts of fluid in the mantle. The lithospheric part of the mantle is too cold to melt but is enriched in fluid compatible elements and [18]O. A metasomatized mantle can be presently involved in arc magmatism by: (1) assimilation of enriched lithospheric mantle by melts from the asthenospheric mantle or (2) partial melting of the enriched lithospheric mantle, caused by the recent intra arc rifting. Cases 1 and 2 suppose an enriched lithospheric mantle below the CKD. A mass balance for ^{18}O, the lack of a strong U–Th disequilibrium and the primitive Pb, Sr and Nd isotopic ratios demand that the time of the mantle metasomatism is at least some Ma but not more than 100 Ma.

ic plate then should favor the flux of ^{18}O-enriched slab fluids into deeper parts of the mantle [32]. The large magma production rate and the observed ^{18}O-enriched compositions in the CKD may all be a consequence of both high fluid input over time and intra-arc extension just where the seamount chain is subducted.

2. It should be easier to trace the process of wedge enrichment for Kamchatka than in other arcs on thick continental crust or with significant sediment subduction.

3. In most arc systems, the magma is mostly derived from the convecting wedge, and a contribution from the subcontinental lithospheric mantle should be minor. Intra-arc rifting in Kamchatka (CKD) may cause that lithospheric mantle regions becomes involved in arc magmatism (Fig. 10).

7. Conclusions

Oxygen isotope ratios of olivines and clinopyroxenes from the Kluchevskoy volcano show distinctly higher values than for MORB. Because assimilation of significant arc crust is ruled out, the observed geochemical and isotopic features must be a characteristic of the arc magma source.

This source is quite different from the MORB-type mantle. Strong positive correlations between $\delta^{18}O$ and fluid mobile major (K, Si) and trace elements (Cs, Li, Sr, Rb, Ba, Th, U, LREE) argue for a depleted mantle source that has exchanged with an isotopically heavy fluid. Sr and Pb are mainly fluid-derived while Nd isotopic compositions represent unmodified mantle. Similarities between Kluchevskoy rocks and the Hawaii plume component in Pb isotopic compositions show that no additional sediment is necessary to explain the slight radiogenic enrichment compared to MORB and that the source for the 'heavy' fluid may be the dehydrating seamount chain.

The large amount of fluid needed clearly argues against a simple fluid-induced melting. Melting and fluid transfer from the slab is de-coupled in time and space. Enrichment of the non-convecting sub-arc lithosphere over at least 10 m.y. is necessary to produce a sufficiently ^{18}O-enriched mantle.

References

[1] T. Plank, C.H. Langmuir, Tracing trace elements from sediment input to volcanic output at subduction zones, Nature 362 (1993) 739–743.

[2] E. Stolper, S. Newman, The role of water in the petrogenesis of Mariana Trough magmas, Earth Planet. Sci. Lett. 121 (1994) 293–325.

[3] J. Ayers, Trace element modeling of aqueous fluid-peridotite interaction in the mantle wedge of subduction zones, Contrib. Mineral. Petrol. 132 (1998) 390–404.

[4] R.S. Harmon, J. Hoefs, Oxygen isotope heterogeneity of the mantle deduced from global ^{18}O systematics of basalts from different geotectonic settings, Contrib. Mineral. Petrol. 120 (1995) 95–114.

[5] D. Mattey, D. Lowry, C. Macpherson, Oxygen isotope composition of mantle peridotite, Earth Planet. Sci. Lett. 128 (1994) 231–241.

[6] J.M. Eiler, K.A. Farley, J.W. Valley, E. Hauri, H. Craig, S.R. Hart, E.M. Stolper, Oxygen isotope variations in ocean island basalt phenocrysts, Geochim. Cosmochim. Acta 61 (1997) 2281–2293.

[7] E. Ito, W.M. White, C. Goepel, The O, Sr, Nd and Pb isotope geochemistry of MORB, Chem. Geol. 62 (1987) 157–176.

[8] F. Pineau, M.P. Semet, N. Grassineau, V.M. Okrugin, M. Javoy, The genesis of the stable isotope (O, H) record in arc magmas: the Kamtchatka's case, Chem. Geol. 135 (1-2) (1999) 93–124.

[9] A.B. Kersting, R.J. Arculus, T.K. Kyser, V.M. Okrugin, A.P. Khrenov, S.A. Fedotov, Klyuchevskoy Volcano, Kamchatka, USSR; geochemical evidence for crustal contamination?, in: W. Compston (Ed.), Seventh International Conference on Geochronology, Cosmochronology and Isotope Geology, Abstracts, Geological Society of Australia 27 (1990) 55, Geological Society of Australia, Sydney, N.S.W.

[10] A.B. Kersting, R.J. Arculus, Klyuchevskoy Volcano, Kamchatka, Russia; the role of high-flux recharged, tapped, and fractionated magma chamber(s) in the genesis of high-Al_2O_3 from high-MgO basalt, J. Petrol. 35 (1994) 1–41.

[11] A.A. Ariskin, G.S. Barmina, A.Y. Ozerov, R.L. Nielsen, Genesis of high-alumina basalts from Kluchevskoi volcano, Petrology 3 (1995) 496–521.

[12] S.A. Fedotov, Y.P. Masurenkov, Active Volcanoes of Kamchatka, Moscow, 1991.

[13] V.B. Piip, Y.A. Yefimova, Seismic sections of the Earth's crust under volcanoes of Kamchatka, Int. Geol. Rev. 35 (1993) 170–177.

[14] Z.D. Sharp, A laser-based microanalytical method for the in situ determination of oxygen isotope ratios of silicates and oxides, Geochim. Cosmochim. Acta 54 (1990) 1353–1357.

[15] M.J. Spicuzza, J.W. Valley, M.J. Kohn, J.P. Girard, A.M. Fouillac, The rapid heating, defocused beam technique; a CO_2-laser-based method for highly precise and accurate determination of delta ^{18}O values of quartz, Chem. Geol. 144 (1998) 195–203.

[16] W. Todt, R.A. Cliff, A. Hanser, A.W. Hofmann, 202Pb-205Pb spike for Pb isotope analysis, Terra Cognita 4 (1984) 209.

[17] A.B. Kersting, R.J. Arculus, Pb isotope composition of Klyuchevskoy Volcano, Kamchatka and North Pacific sediments; implications for magma genesis and crustal recycling in the Kamchatkan arc, Earth Planet. Sci. Lett. 136 (1995) 133–148.

[18] S.A. Khubunaya, S.O. Bogoyavlenskiy, T.Y. Novogorodtseva, A.I. Okrugina, The mineralogy of the Kluchevskoi magnesian basalts depicting the fractionation in the magma chamber, Volcanol. Seismol. 15 (1994) 315–338.

[19] Y.F. Zheng, Calculation of oxygen isotope fractionation in anhydrous silicate minerals, Geochim. Cosmochim. Acta 57 (1993) 1079–1091.

[20] G. Website, http://www-ep.es.llml.gov/germ/partitioning.html#Ds

[21] J.M. Eiler, K.A. Farley, J.W. Valley, A.W. Hofmann, E.M. Stolper, Oxygen isotope constraints on the sources of Hawaiian volcanism, Earth Planet. Sci. Lett. 144 (1996) 453–468.

[22] P.F. Dobson, J.R. O'Neil, Stable isotope compositions and water contents of boninite series volcanic rocks from Chichi-jima, Bonin Islands, Japan, Earth Planet. Sci. Lett. 82 (1987) 75–86.

[23] D. Rea, I.A. Basov, L.A. Krissek, Leg 145 Scientific party, Scientific results odf drilling the North Pacific transect, Proceedings of the Ocean Drilling Program, Scientific Results 145 (1995) 577–595.

[24] J.C. Bailey, Role of subducted sediments in the genesis of Kurile-Kamchatka island arc basalts; Sr isotopic and elemental evidence, Geochem. J. 30 (1996) 289–321.

[25] H. Staudigel, T. Plank, B. White, H.U. Schmincke, Geochemical fluxes during seafloor alteration of the basaltic upper oceanic crust; DSDP sites 417 and 418, in: G.E. Bebout, D.W. Scholl, S.H. Kirby, J.P. Platt (Eds.), Subduction Top to Bottom, Geophysical Monograph 96 (1996) 19–38, American Geophysical Union, Washington, DC.

[26] J.M. Brenan, H.F. Shaw, F.J. Ryerson, D.L. Phinney, Mineral-aqueous fluid partitioning of trace elements at 900 degrees C and 2.0 GPa; constraints on the trace element chemistry of mantle and deep crustal fluids, Geochim. Cosmochim. Acta 59 (1995) 3331–3350.

[27] R. Stalder, S.F. Foley, G.P. Brey, I. Horn, Mineral-aqueous fluid partitioning of trace elements at 900°C–1200°C and 3.0 GPa to 5.7 GPa new experimental data for garnet clinopyroxene and rutile and implications for mantle metasomatism, Geochim. Cosmochim. Acta 62 (1998) 1781–1801.

[28] M.T. McCulloch, V.C. Bennett, Progressive growth of the Earth's continental crust and depleted mantle; geochemical constraints, Geochim. Cosmochim. Acta 58 (1994) 4717–4738.

[29] T. Elliott, T. Plank, A. Zindler, W. White, B. Bourdon,

Element transport from slab to volcanic front at the Mariana Arc, J. Geophys. Res. B Solid Earth Planets 102 (1997) 14991–15019.

[30] S. Turner, F. McDermott, C. Hawkesworth, P. Kepezhinskas, A U-series study of lavas from Kamchatka and the Aleutians: constraints on source composition and melting processes, Contrib. Mineral. Petrol. 133 (1998) 217–234.

[31] O. Navon, E. Stolper, Geochemical consequences of melt percolation; the upper mantle as a chromatographic column, J. Geol. 95 (1987) 285–307.

[32] S.M. Peacock, Large-scale hydration of the lithosphere above subducting slabs, in: J.L.R. Touret, A.B. Thompson (Eds.), Fluid-Rock Interaction in the Deeper Continental Lithosphere, Chem. Geol. 108 (1993) 49–59, Elsevier, Amsterdam.

[33] S.S. Sorensen, J.N. Grossman, M.R. Perfit, Phengite-hosted LILE enrichment in eclogite and related rocks; implications for fluid-mediated mass transfer in subduction zones and arc magma genesis, J. Petrol. 38 (1997) 3–34.

[34] R. Tribuzio, B. Messiga, R. Vannucci, P. Bottazzi, Rare earth element redistribution during high-pressure-low-temperature metamorphism in ophiolitic Fe-gabbros (Liguria, northwestern Italy); implications for light REE mobility in subduction zones, Geology (Boulder) 24 (1996) 711–714.

[35] G.E. Bebout, The impact of subduction-zone metamorphism on mantle-ocean chemical cycling, in: H. Staudigel, F. Albarede, D. Hilton, T. Elliott (Eds.), The Mantle-Ocean Connection, Chem. Geol. 126 (1995) 191–218, Elsevier, Amsterdam.

[36] G.E. Bebout, M.D. Barton, Metasomatism during subduction; products and possible paths in the Catalina Schist, California, in: J.L.R. Touret, A.B. Thompson (Eds.), Fluid-Rock Interaction in the Deeper Continental Lithosphere, Chem. Geol. 108 (1993) 61–92, Elsevier, Amsterdam.

[37] J.M. Eiler, B. McInnes, J.W. Valley, C.M. Graham, E.M. Stolper, Oxygen isotope evidence for slab-derived fluids in the sub-arc mantle, Nature 393 (1998) 777–781.

[38] M.T. McCulloch, A.J. Gamble, Geochemical and geodynamical constraints on subduction zone magmatism, Earth Planet. Sci. Lett. 102 (1991) 358–374.

[39] A.W. Hofmann, Chemical differentiation of the Earth; the relationship between mantle, continental crust, and oceanic crust, in: E. Welin (Ed.), Isotope Geochemistry; The Crafoord Symposium, Earth Planet. Sci. Lett. 90 (1988) 297–314, Elsevier, Amsterdam.

[40] J.C. Ayers, S.K. Dittmer, G.D. Layne, Partitioning of elements between peridotite and H_2O at 2.0–3.0 GPa and 900–1100 degrees C, and application to models of subduction zone processes, Earth Planet. Sci. Lett. 150 (1997) 381–398.